



Significance of hyperintense arteries on Gd-enhanced 3D T1W black-blood imaging in acute stroke

Kyung-Yul Lee^{1,2} · Sang Hyun Suh³ · Sung Jun Ahn³

Received: 11 April 2018 / Revised: 18 June 2018 / Accepted: 13 July 2018 / Published online: 7 August 2018
© European Society of Radiology 2018

Abstract

Objectives To elucidate the pathogenesis of hyperintense arteries on Gd-enhanced 3D T1W BB FSE and their clinical significance in acute middle cerebral artery (MCA) stroke.

Methods We retrospectively reviewed 20 patients with MCA infarction. We measured the contrast-to-noise ratio between hyperintense artery and adjacent grey matter on T2-FLAIR and Gd-enhanced 3D T1W BB FSE and compared them by using Student's *t* test. The agreement of positive hyperintense artery between T2 FLAIR and Gd-enhanced 3D T1WI BB FSE was estimated with intraclass correlation coefficient. Our cohort was dichotomised into two groups depending on hyperintense artery scores, and clinical data were compared between two groups by using Student's *t* test and chi-square test.

Results The contrast between hyperintense artery and grey matter on Gd-enhanced 3D T1W BB FSE was significantly higher than that on T2-FLAIR (2.27 ± 1.65 versus 0.94 ± 0.86 , $p = 0.01$). Overall, agreement of hyperintense arteries on T2-FLAIR and Gd-enhanced 3D T1W BB FSE was excellent ($\rho = 0.76$, $p < 0.01$). Patients with higher hyperintense artery scores had higher perfusion deficits than those with lower hyperintense artery scores (196.7 ± 41.4 vs 100.1 ± 130.1 , $p = 0.03$).

Conclusion Hyperintense arteries on Gd-enhanced 3D T1W BB FSE in acute MCA stroke may be associated with slow collateral flows. Their territories corresponded to those of FLAIR, but had a better contrast. The patients with hyperintense arteries in a wider territory showed larger perfusion deficit than those with hyperintense arteries in a narrower territory.

Key Points

- Hyperintense arteries on Gd-enhanced 3D T1W BB FSE are slow collateral flows.
- Hyperintense arteries on Gd-enhanced 3D T1W BB FSE are well matched with FLAIR hyperintense vessels.
- Hyperintense arteries are associated with perfusion deficit in stroke patients.

Keywords Arteries · Magnetic resonance imaging · Stroke

Abbreviations

| | |
|---------------|--|
| 3D T1W BB FSE | Three-dimensional T1-weighted black-blood fast spin echo |
| ASPECTS | Alberta stroke program early CT score |
| CSF | Cerebrospinal fluid |
| FLAIR | Fluid attenuated inversion recovery |

| | |
|-------|--|
| Gd | Gadolinium |
| ICA | Internal carotid artery |
| MCA | Middle cerebral artery |
| mRS | Modified Rankin scale |
| NIHSS | National Institutes of Health Stroke Scale |

✉ Sung Jun Ahn
aahng77@yuhs.ac

¹ Department of Neurology, Gangnam Severance Hospital, Yonsei University College of Medicine, 211 Eonju-ro, Gangnam-gu, Seoul 06273, Korea

² Severance Institute for Vascular and Metabolic Research, Yonsei University, Seoul, Korea

³ Department of Radiology, Gangnam Severance Hospital, Yonsei University College of Medicine, 211 Eonju-ro, Gangnam-gu, Seoul 06273, Korea

Introduction

Traditional catheter angiography and noninvasive luminal imaging techniques (MR angiography or CT angiography) can only identify abnormalities affecting vessel lumen [1, 2]. However, high-resolution black-blood images allow direct characterisation of vessel wall status in the setting of acute stroke. Intracranial artery atherosclerosis, dissection, moyamoya disease, vasculitis and reversible cerebral

vasoconstriction syndrome can be diagnosed and differentiated by using high-resolution black-blood images [1, 3–9].

A variety of black-blood imaging techniques have been developed. 3D variable refocusing flip angle sequences (VISTA, Philips Healthcare, Best, the Netherlands; SPACE, Siemens Healthcare, Erlangen, Germany; CUBE, GE Healthcare, Milwaukee, USA) have been the most extensively studied 3D techniques to date, as these sequences provide blood suppression as well as excellent image quality and increased coverage in a shorter scan time [10–13]. Recently, additional blood suppression techniques have been employed with 3D variable refocusing flip angle. One such technique is motion-sensitised driven equilibrium, which uses flow-sensitive dephasing gradients to suppress flow [14–16]. Another technique is the delay alternating with nutation for tailored excitation pulse train, which uses a series of low flip angle non-selective pulses interleaved with gradient pulses with short repetition times that can result in both optimised blood and cerebrospinal fluid (CSF) suppression, without any effects on tissue contrast [17].

As 3D high-resolution black-blood images have been widely used, hyperintense arteries are frequently encountered on Gd-enhanced three-dimensional T1-weighted black-blood fast spin echo (3D T1W BB FSE) images in patients with stroke. We presume that this sign is associated with collateral sluggish flow in acute stroke, but none of the previous studies have revealed this phenomenon and evaluated its clinical impact. Various imaging techniques are used in acute stroke. CT angiography detects intracranial stenosis and occlusion site with high sensitivity (97–100%) and specificity (98–100%) [18, 19]. Digital subtraction angiography (DSA) is considered as the reference standard for detection of stenosis and occlusion. Fluid attenuated inversion recovery (FLAIR) hyperintense vessels reflect sluggish collateral flows [20–22]. They are strongly related to proximal large-vessel occlusion or severe stenosis [23, 24]. Recently, clinical application of FLAIR hyperintense vessels has been actively studied but not yet concluded [25, 26]. Perfusion images are not used to select patients for intravenous thrombolysis [27]. However, they may identify the salvageable brain parenchyma for newer therapy or treatment outside accepted time windows [28–30]. Moreover, perfusion images may predict a patient's clinical outcome, detect the additional vascular territories at risk that may be otherwise normal on conventional imaging and differentiate stroke from its mimics [31–33]. Thus, in this study, by comparing these various imaging techniques, we might be able to elucidate the pathogenesis of hyperintense artery on 3D T1W BB FSE and its clinical significance in acute middle cerebral artery (MCA) stroke.

Materials and methods

Patients

We retrospectively screened consecutive patients who presented to our tertiary referral medical centre between January 2017 and December 2017. We included patients with acute MCA territory ischaemic stroke within 1 week of symptom onset. They all underwent stroke MR imaging. All of the patients included in the study showed restricted diffusion in the MCA territory on diffusion-weighted imaging. We excluded patients with transient ischaemic attack, multiple infarctions other than in MCA territories, or lacunar infarction. Our institutional review board approved this retrospective study. The following cerebrovascular risk factors were evaluated on admission: smoking, arterial hypertension, diabetes mellitus and hyperlipidaemia. Stroke severity was assessed by using the National Institutes of Health Stroke Scale (NIHSS). Functional outcome was assessed 3 months post-stroke by using the modified Rankin scale (mRS) score: favourable outcome was defined as mRS score of 2 or less. Arterial occlusions were categorised into proximal Internal carotid artery (ICA), distal ICA, MCA horizontal segment, MCA insular segment and MCA cortical segment.

Imaging protocols

All patients underwent both brain CT angiography (SOMATOM Definition AS+, Siemens Healthcare, Forchheim, Germany) and brain 3-T MRI (Discovery MR750; GE Healthcare, Milwaukee, USA). The brain CT angiography protocol included 1-mm non-

Table 1 Baseline characteristics and MRA findings of patients

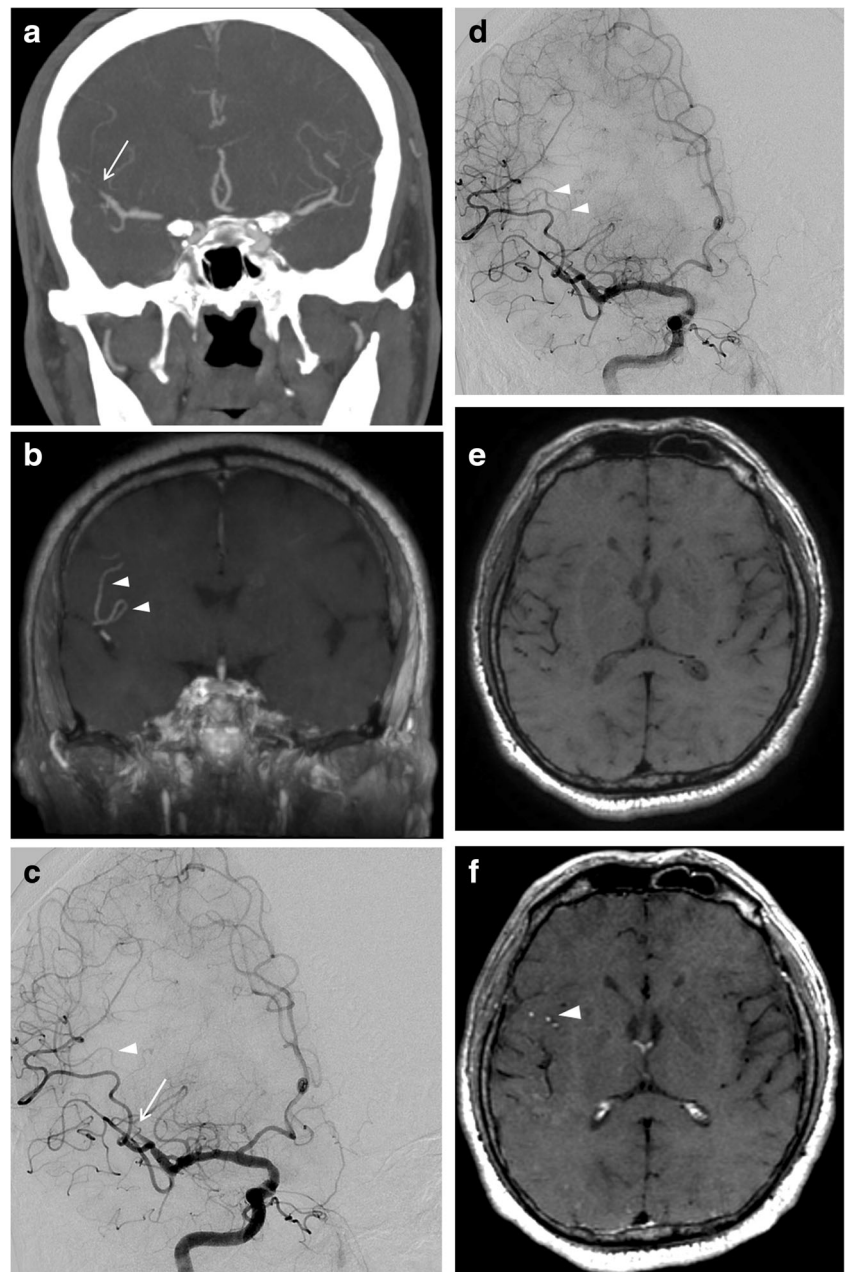
| Features | |
|--|---------------|
| No. of patients | 20 |
| Age (years) (mean) (SD) | 69.5 (9.7) |
| Female (no.) (%) | 5 (25) |
| Hypertension (no.) (%) | 11 (55) |
| Diabetes mellitus (no.) (%) | 8 (40) |
| Hyperlipidaemia (no.) (%) | 6 (30) |
| Current smoking (no.) (%) | 6 (30) |
| NIHSS score (median) (IQR) | 11 (5.5–16.5) |
| Onset-to-MRI time (min) (median) (IQR) | 360 (235–580) |
| Occlusion site | |
| MCA horizontal segment | 5 (25) |
| MCA insular segment | 5 (25) |
| MCA cortical segment | 4 (20) |
| Distal ICA | 0 |
| Proximal ICA | 6 (30) |

ICA Internal carotid artery, IQR interquartile range, SD standard deviation

contrast CT and CT angiography with the same thickness. The maximum intensity projection using source data was obtained. Our stroke MR imaging protocol for acute stroke included DWI and T2-FLAIR. In addition, dynamic susceptibility contrast (DSC) perfusion-weighted imaging and 3D T1W BB FSE were acquired sequentially after administration of a compact bolus (0.1 mmol/kg) of gadobutrol at an injection rate of 5 mL/s. The parameters for DWI were repetition time (TR)/echo time (TE) = 8000/65.6 ms; slice thickness = 3 mm; gap = 0.1 mm; matrix size = 160×160 ; field of view (FOV) = $240 \times 240 \text{ mm}^2$; three directions; b value = 0 and 1000 s/mm^2 . T2-FLAIR images were acquired with the following parameters: TR/TE = 12,000/140 ms; inversion time (TI) = 2500 ms; slice thickness = 4 mm;

gap = 1 mm; flip angle = 110° ; FOV = $210 \times 210 \text{ mm}^2$; matrix = 352×353 ; and 30 contiguous sections for a total acquisition of 3 min 20 s. DSC perfusion MRI employed gradient echo-planar imaging and imaging parameters were TR/TE = 1500/23 ms; slice thickness = 4 mm; gap = 1 mm; flip angle = 60° ; FOV = $220 \times 220 \text{ mm}^2$; matrix = 100×100 . The acquisition time was 1 min 40 s. To obtain 3D T1W BB FSE, motion-sensitized driven equilibrium prepared pulse was added in the front of 3D T1W FSE with variable flip angle. The scan parameters of 3D T1W FSE with variable flip angle were TR/TE = 500/24.5 ms; slice thickness = 1 mm; echo train length = 24; flip angle = variable; FOV = $220 \times 220 \text{ mm}^2$; matrix = 256×224 ; 170 axial slices. The acquisition time was 4 min 50 s.

Fig. 1 **a** Maximum intensity projection image of CT angiography shows occlusion in the right MCA, insular segment (arrow). **b** Maximum intensity projection image of Gd-enhanced 3D T1W BB FSE shows hyperintense arteries (arrowheads) distal to the occlusion site. **c** Angiography in early phase shows occlusion in the right MCA, insular segment. **d** Retrograde collateral flow is filled in the delayed phase at the region where the hyperintense artery is seen. Hyperintense artery is not seen on the pre-contrast (**e**) but on the post-contrast 3D T1W BB FSE (**f**)



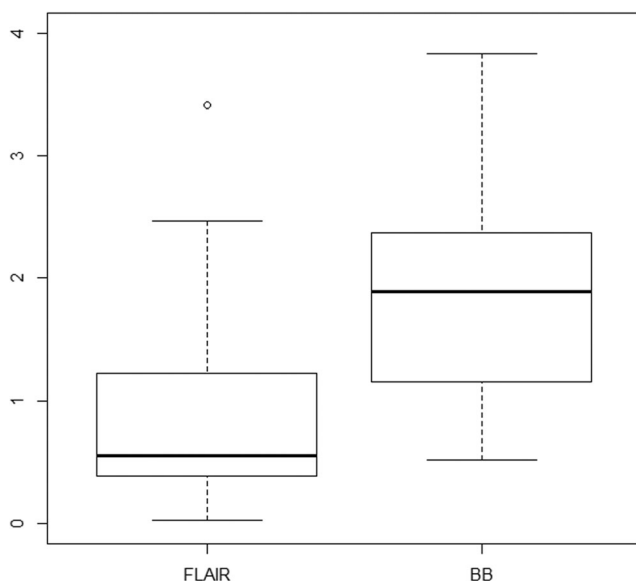


Fig. 2 Boxplots of contrast-to-noise and artery-to-grey matter ratios for FLAIR and Gd-enhanced 3D T1W BB FSE

Image analysis

Multimodality images of patients (CT angiography, cerebral angiography, advanced MRI) were reviewed to elucidate the pathogenesis of hyperintense arteries on Gd-enhanced 3D T1W BB FSE.

Two readers independently assessed either T2-FLAIR or Gd-enhanced 3D T1W BB FSE. The first review of images was randomly selected by the study coordinator. The remaining sequences were reviewed 1 week later. The reviewers were blinded to clinical history. Hyperintense arteries were defined as focal, tubular or serpentine hyperintensities in subarachnoid spaces with a typical arterial course of at least two consecutive axial sections of each of the seven Alberta Stroke Program Early CT Score (ASPECTS) territories (insula, M1–M6) [34]. An ASPECTS cortical area was considered positive when it coincided with hyperintense arteries. Hyperintense artery scores were defined as the total number of positive ASPECTS cortical areas on Gd-enhanced 3D T1W BB FSE.

To compare artery-to-grey matter contrast on both sequences, we calculated the contrast-to-noise ratio between hyperintense arteries and adjacent grey matter. The contrast-to-noise ratio was defined as $(SI_{\text{artery}} - SI_{\text{GM}})/(SD_{\text{artery}}^2 + SD_{\text{GM}}^2)^{1/2}$, where SI_{artery} and SI_{GM} are signal intensities of hyperintense artery and adjacent grey matter respectively. SD_{artery} and SD_{GM} denote standard deviation of hyperintense artery and adjacent grey matter respectively [35].

The ischaemic lesion volume and perfusion abnormality volume were also measured as follows: DWI images were coregistered to T_{max} of the perfusion map using FMRIB Software Library tools (FSL, Version 5.0; [https://fsl.fmrib.](https://fsl.fmrib.ox.ac.uk/fsl)

[ox.ac.uk/fsl](https://fsl.fmrib.ox.ac.uk/fsl)). The free open-source toolkit ITK-SNAP (www.itksnap.org) was used for drawing regions of interest (ROIs). Two different reviewers drew ROIs separately along the borders of the high-signal area on registered DWI and yellow territories on coloured T_{max} maps ($T_{\text{max}} > 6$ s). The T_{max} map was generated by using perfusion-processing software (Func-tool; GE Healthcare). Infarct growth was defined as DWI lesion volume after thrombolysis minus DWI baseline lesion volume.

Statistical analysis

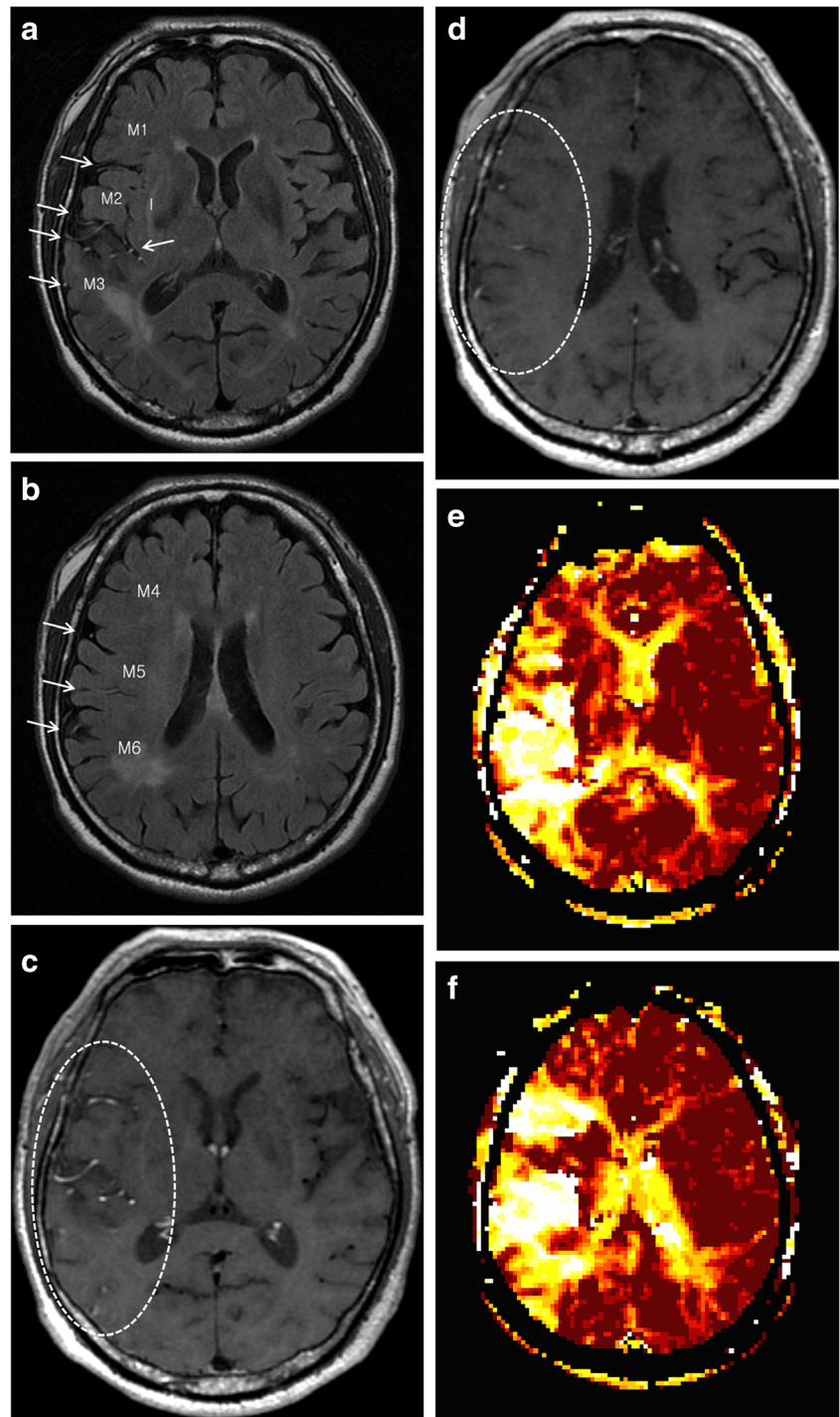
Artery-to-grey matter contrasts on T2-FLAIR and Gd-enhanced 3D T1W BB FSE were compared by using Student's *t* test. The agreement of hyperintense arteries on both sequences according to each MCA ASPECTS territory was estimated with the intraclass correlation coefficient using the two-way random effects model. Using an accepted standard, we defined intraclass correlation coefficient values below 0.40 as poor, between 0.40 and 0.59 as fair, between 0.60 and 0.74 as good, and over 0.74 as excellent [36]. Interobserver agreement of volume measurement was also performed with same method as above. Our cohort was dichotomised into two groups using median hyperintense artery scores (hyperintense artery score < 5 vs ≥ 5). We further compared clinical and imaging data (age, sex, hypertension, diabetes mellitus, hyperlipidaemia, smoking status, NIHSS score, baseline infarct volume, infarct growth, perfusion deficit and favourable outcome) between the two groups by using Student's *t* test and chi-square test. All statistical analysis was performed by using Statistical Package for Social Sciences (SPSS) software (version 21, IBM Corp., Armonk, NY, USA). *P* values less than 0.05 were considered statistically significant.

Results

Baseline characteristics

Twenty patients fulfilled the inclusion criteria (Table 1). The mean age was 69.5 years, and 25% of patients were women. Eleven patients (50%) had hypertension, eight patients (40%) had diabetes mellitus, six patients (30%) had hyperlipidaemia, and six patients (30%) were current smokers. The median initial NIHSS score was 11 (interquartile range, 5.5–16.5). The median time from symptom onset to MR imaging was 360 min (interquartile range, 235–580 min). Occlusion sites included the following areas: the MCA horizontal segment (5/20, 25%), MCA insular segment (5/20, 25%), MCA cortical segment (4/20, 20%) and the proximal ICA (6/20, 30%).

Fig. 3 A 66-year-old man with right MCA territory infarction. Arterial hyperintensities are seen in the Sylvian fissure, M2, M3, M5 and M6 on T2-FLAIR (a, b), and they are well matched with those on Gd-enhanced 3D T1W BB FSE (c, d). T_{max} is prolonged in the corresponding regions (e, f)



Illustrative case of arterial hyperintensity with multimodality images

A 62-year-old man presented with left-sided weakness with an initial NIHSS score of 10. CT angiography and digital subtraction angiography showed occlusion in the right MCA, insular segment. Hyperintense artery was

visualised distal to the occlusion site on post-contrast 3D T1W BB FSE, and not on the pre-contrast study. The velocity of hyperintense artery appeared to be slower than that of the vein, since the signal intensity of the posterior superior sagittal sinus was suppressed. Hyperintense artery was well matched with the retrograde collateral flow on digital subtraction angiography (Fig. 1).

Table 2 Agreement between hyperintense arteries on FLAIR and Gd-enhanced 3D T1W BB FSE according to each ASPECTS territory

| ASPECTS territories | Inter-sequence agreement | <i>p</i> value |
|---------------------|--------------------------|----------------|
| Whole territories | 0.76 | < 0.01 |
| I | 0.87 | < 0.01 |
| M1 | 0.8 | < 0.01 |
| M2 | 0.78 | < 0.01 |
| M3 | 0.81 | < 0.01 |
| M4 | 0.79 | < 0.01 |
| M5 | 0.67 | 0.01 |
| M6 | 0.56 | 0.04 |

Comparison with hyperintense artery on T2-FLAIR

The contrast-to-noise ratio between the hyperintense artery and adjacent grey matter on Gd-enhanced 3D T1W BB FSE was significantly higher than that on T2-FLAIR (2.27 ± 1.65 versus 0.94 ± 0.86 , $p = 0.01$, Fig. 2).

Overall, agreement of hyperintense arteries on T2-FLAIR and Gd-enhanced 3D T1W BB FSE was excellent ($\rho = 0.76$, $p < 0.01$, Fig. 3). Regarding each ASPECT territory, agreements were excellent in I, M1, M2, M3 and M4 ($\rho = 0.87, 0.8, 0.78, 0.81$ and 0.79 respectively, $p < 0.01$), good in M5 ($\rho = 0.67$, $p = 0.01$) and fair in M6 ($\rho = 0.56$, $p = 0.04$) (Table 2).

Clinical significance of hyperintense artery on Gd-enhanced 3D T1W BB FSE

Interobserver agreements for volume measurement of DWI and perfusion images were excellent ($\rho = 0.99$, $p < 0.01$). Patients with higher hyperintense artery scores had higher perfusion deficits than those with lower hyperintense artery scores (196.7 ± 41.4 vs 100.1 ± 130.1 , $p = 0.03$) (Table 3).

Age, sex, hypertension, diabetes mellitus, hyperlipidaemia, current smoking, NIHSS score, baseline infarct volume, infarct growth and favourable outcome were not significantly different between the two groups.

Discussion

This study showed that in patients with acute MCA stroke, the hyperintense artery sign on Gd-enhanced 3D T1W BB FSE may have resulted from a retrograde slow collateral flow and was well matched with the FLAIR hyperintense vessel sign, but showed a better contrast. The patients with hyperintense artery in a wider territory showed higher perfusion deficit than those with hyperintense artery in a narrower territory.

Gd-enhanced high-resolution black-blood T1-weighted imaging has been commonly used in stroke, and Jang et al showed that it improves detection of intraluminal thrombi [37]. However, hyperintense artery signs are rarely mentioned [13, 38–40]. Hui et al first mentioned the hyperintense artery sign as a “white snake sign” and they presumed that this sign may be due to a sluggish slow flow and just distal to a thrombus [41]. Our results agree with those of the previous study. Hyperintense artery corresponds to a sluggish collateral flow. This retrograde slow flow may result in loss of the flow void phenomenon, and vessels may appear hyperintense against the dark CSF background [42, 43]. However, according to our results, a collateral flow did not appear hyperintense on non-enhanced 3D T1W BB FSE. This implies that the appearance of hyperintense artery cannot be explained only by loss of the flow void phenomenon. We presume that the T1-shortening effect of Gd contributes to the underlying loss of the flow void phenomenon, making sluggish flows hyperintense.

Table 3 Comparison of baseline parameters and clinical outcome based on the number of hyperintense artery scores

| | Hyperintense artery scores < 5 | Hyperintense artery scores ≥ 5 | <i>p</i> value |
|--|--------------------------------|-------------------------------------|----------------|
| No. | 8 | 12 | |
| Age (years) (mean) (SD) | 71.1 (10.7) | 68.5 (9.2) | 0.56 |
| Female (no.) (%) | 2 (25) | 3 (25) | 0.21 |
| Hypertension (no.) (%) | 5 (62.5) | 6 (50) | 0.58 |
| Diabetes mellitus (no.) (%) | 3 (37.5) | 5 (41.6) | 0.49 |
| Hyperlipidaemia (no.) (%) | 3 (37.5) | 3 (25) | 0.42 |
| Current smoking (no.) (%) | 2 (25) | 4 (33.3) | 0.88 |
| NIHSS score (mean) (SD) | 10.3(7.3) | 12.3(5.1) | 0.48 |
| Baseline infarct volume (mL) (mean) (SD) | 39.0 (37.4) | 50.5 (58.5) | 0.71 |
| Infarct growth (mean) (SD) | 20.3 (41.0) | 23.4 (20.5) | 0.87 |
| Perfusion deficit (mL) (mean) (SD) | 100.1 (130.1) | 196.7 (41.4) | 0.03 |
| Favourable outcome at 3 months (no.) (%) | 5 (62.5) | 5 (41.6) | 0.81 |

Hyperintense artery is more prominent on Gd-enhanced 3D T1W BB FSE than on T2-FLAIR. The signal intensity of GM is lower than that of WM on T1WI, whereas the signal intensity of GM is higher than that of WM on T2-FLAIR [44, 45]. Thus, the contrast between hyperintense artery and adjacent grey matter was not distinct on T2-FLAIR. Overall, the regions of hyperintense artery distribution were well matched with those on T2-FLAIR. However, the degree of agreement between two sequences was decreased in M5 and M6, compared to other ASPECTS territories (I, M1, M2, M3, M4). Previous studies have reported that hyperintense artery on T2-FLAIR is prominent within the Sylvian fissure [23, 46, 47]. This might be because larger arteries have a slower flow speed than smaller distal arteries under the same perfusion pressure. Likewise, in our results, hyperintense artery on T2-FLAIR tended not to be observed in distal cortical regions (M4, M5 and M6), which may explain the slight discrepancy between the two sequences.

The clinical significance of hyperintense artery on Gd-enhanced 3D T1W BB FSE has not been reported. According to our results, in most territories, the greater the hyperintensity of the artery was, the larger the perfusion deficit was. However, the extent of hyperintense artery was not related to baseline infarct volume, infarct growth and patient outcome. Considering the similarities of hyperintense artery on Gd-enhanced 3D T1W BB FSE with that on T2-FLAIR regarding pathogenesis and extent, we suggest its clinical significance. Previous papers have frequently stated the association of FLAIR hyperintense vessels with large perfusion lesions and bigger mismatch volumes [23, 46, 48–50]. However, in determining the prognostic information provided by FLAIR hyperintense vessels, the data are seemingly contradictory. Some authors have noted that the presence of FLAIR hyperintense vessels is correlated with smaller infarct volume and better clinical outcomes [25, 51]. In contrast to these studies, Kufner et al observed that the presence of FLAIR hyperintense vessels was associated with larger perfusion deficits, larger growth and more severe hypoperfusion [26]. One reason for these differences may be that FLAIR hyperintense vessels imply a mixture of “poor” and “good” collaterals, hampering the differentiation between true penumbra and benign oligoemia [50]. Moreover, the occlusion sites in our cohort were heterogeneous. Specifically, patients’ outcomes may be different depending on occlusion site [52]. The clinical significance of hyperintense artery on Gd-enhanced 3D T1W BB FSE should be further investigated in future studies with larger cohorts and consistent occlusion sites.

In addition, application of new techniques may affect the extent of hyperintense artery. The Periodically Rotated Overlapping Parallel Lines with Enhanced Reconstruction (PROPELLER) technique increases the extent of FLAIR hyperintense artery and its territory is more related to perfusion abnormality than that of conventional FLAIR [20]. Thus, there is a chance that other black-blood techniques such as

Delay Alternating with Nutation for Tailored Excitation (DANTE) may change the extent of hyperintense artery.

Recently, some studies demonstrated a strong correlation between susceptibility-weighted imaging (SWI) and perfusion imaging, and they proposed that asymmetrical dilated vessel-like signal loss in the cortex on SWI could be a marker of penumbra [53, 54]. This sign on SWI may reflect the haemodynamic changes resulting from the dilatation of vessels in response to ischaemia and an elevated oxygen extraction fraction (OEF) following an increase of the ratio of deoxyhaemoglobin to oxyhaemoglobin [55]. Thus, it might be interesting to evaluate the relationship between hyperintense artery on black-blood images and dark vessels on SWI.

There was a limitation in our study. The number of cases was small and might not be sufficient to make a solid conclusion regarding its clinical significance. However, various imaging modalities clearly show that hyperintense artery on Gd-enhanced 3D T1 BB FSE is a sluggish collateral flow. We also believe that our preliminary results supporting its clinical significance may serve as a cornerstone for future studies with a larger population to validate and extend these results.

Conclusion

Hyperintense arteries on Gd-enhanced 3D T1W BB FSE in acute MCA stroke may be associated with a retrograde slow collateral flow. Their territories corresponded to those of FLAIR, but had a better contrast. The patients with hyperintense arteries in a wider territory showed larger perfusion deficit than those with hyperintense arteries in a narrower territory. However, their clinical significance should be further studied with larger and homogenous cohorts.

Funding The authors state that this work has not received any funding.

Compliance with ethical standards

Guarantor The scientific guarantor of this publication is Kyung-Yul Lee.

Conflict of interest The authors of this manuscript declare no relationships with any companies whose products or services may be related to the subject matter of the article.

Statistics and biometry No complex statistical methods were necessary for this paper.

Informed consent Written informed consent was waived by the institutional review board.

Ethical approval Institutional review board approval was obtained.

Methodology

- retrospective
- diagnostic or prognostic study
- performed at one institution

References

- Kim YJ, Lee DH, Kwon JY et al (2013) High resolution MRI difference between moyamoya disease and intracranial atherosclerosis. *Eur J Neurol* 20:1311–1318
- Natori T, Sasaki M, Miyoshi M et al (2014) Evaluating middle cerebral artery atherosclerotic lesions in acute ischemic stroke using magnetic resonance T1-weighted 3-dimensional vessel wall imaging. *J Stroke Cerebrovasc Dis* 23:706–711
- Choi YJ, Jung SC, Lee DH (2015) Vessel wall imaging of the intracranial and cervical carotid arteries. *J Stroke* 17:238–255
- Saam T, Habs M, Pollatos O et al (2010) High-resolution black-blood contrast-enhanced T1 weighted images for the diagnosis and follow-up of intracranial arteritis. *Br J Radiol* 83:e182–e184
- Saam T, Hatsukami TS, Takaya N et al (2007) The vulnerable, or high-risk, atherosclerotic plaque: noninvasive MR imaging for characterization and assessment. *Radiology* 244:64–77
- Bley TA, Wieben O, Uhl M, Thiel J, Schmidt D, Langer M (2005) High-resolution MRI in giant cell arteritis: imaging of the wall of the superficial temporal artery. *AJR Am J Roentgenol* 184:283–287
- Takano K, Hida K, Kuwabara Y, Yoshimitsu K (2017) Intracranial arterial wall enhancement using gadolinium-enhanced 3D black-blood T1-weighted imaging. *Eur J Radiol* 86:13–19
- Ben Hassen W, Machet A, Edjlali-Goujon M et al (2014) Imaging of cervical artery dissection. *Diagn Interv Imaging* 95:1151–1161
- Obusez EC, Hui F, Hajji-Ali RA et al (2014) High-resolution MRI vessel wall imaging: spatial and temporal patterns of reversible cerebral vasoconstriction syndrome and central nervous system vasculitis. *AJNR Am J Neuroradiol* 35:1527–1532
- Busse RF, Brau AC, Vu A et al (2008) Effects of refocusing flip angle modulation and view ordering in 3D fast spin echo. *Magn Reson Med* 60:640–649
- Kato Y, Higano S, Tamura H et al (2009) Usefulness of contrast-enhanced T1-weighted sampling perfection with application-optimized contrasts by using different flip angle evolutions in detection of small brain metastasis at 3T MR imaging: comparison with magnetization-prepared rapid acquisition of gradient echo imaging. *AJNR Am J Neuroradiol* 30:923–929
- Fan Z, Zhang Z, Chung YC et al (2010) Carotid arterial wall MRI at 3T using 3D variable-flip-angle turbo spin-echo (TSE) with flow-sensitive dephasing (FSD). *J Magn Reson Imaging* 31:645–654
- Qiao Y, Zeiler SR, Mirbagheri S et al (2014) Intracranial plaque enhancement in patients with cerebrovascular events on high-spatial-resolution MR images. *Radiology* 271:534–542
- Korosec FR, Grist TM, Polzin JA, Weber DM, Mistretta CA (1993) MR angiography using velocity-selective preparation pulses and segmented gradient-echo acquisition. *Magn Reson Med* 30:704–714
- Norris DG, Schwarzbauer C (1999) Velocity selective radiofrequency pulse trains. *J Magn Reson* 137:231–236
- Zhu C, Graves MJ, Yuan J, Sadat U, Gillard JH, Patterson AJ (2014) Optimization of improved motion-sensitized driven-equilibrium (iMSDE) blood suppression for carotid artery wall imaging. *J Cardiovasc Magn Reson* 16:61
- Wang J, Helle M, Zhou Z, Bornert P, Hatsukami TS, Yuan C (2016) Joint blood and cerebrospinal fluid suppression for intracranial vessel wall MRI. *Magn Reson Med* 75:831–838
- Shrier DA, Tanaka H, Numaguchi Y, Konno S, Patel U, Shibata D (1997) CT angiography in the evaluation of acute stroke. *AJNR Am J Neuroradiol* 18:1011–1020
- Nguyen-Huynh MN, Wintermark M, English J et al (2008) How accurate is CT angiography in evaluating intracranial atherosclerotic disease? *Stroke* 39:1184–1188
- Ahn SJ, Suh SH, Lee KY, Kim JH, Seo KD, Lee S (2015) Hyperintense vessels on T2-PROPELLER-FLAIR in patients with acute MCA stroke: prediction of arterial stenosis and perfusion abnormality. *AJNR Am J Neuroradiol* 36:2042–2047
- Lee SH, Seo KD, Kim JH, Suh SH, Ahn SJ, Lee KY (2016) Correlation between hyperintense vessels on FLAIR imaging and arterial circulation time on cerebral angiography. *Magn Reson Med* 15:105–110
- Ahn SJ, Lee KY, Ahn SS, Suh H, Kim BS, Lee SK (2016) Can FLAIR hyperintense vessel (FHV) signs be influenced by varying MR parameters and flow velocities? A flow phantom analysis. *Acta Radiol* 57:580–586
- Kamran S, Bates V, Bakshi R, Wright P, Kinkel W, Miletich R (2000) Significance of hyperintense vessels on FLAIR MRI in acute stroke. *Neurology* 55:265–269
- Cosnard G, Duprez T, Grandin C, Smith AM, Munier T, Peeters A (1999) Fast FLAIR sequence for detecting major vascular abnormalities during the hyperacute phase of stroke: a comparison with MR angiography. *Neuroradiology* 41:342–346
- Lee KY, Latour LL, Luby M, Hsia AW, Merino JG, Warach S (2009) Distal hyperintense vessels on FLAIR: an MRI marker for collateral circulation in acute stroke? *Neurology* 72:1134–1139
- Kufner A, Galinovic I, Ambrosi V et al (2015) Hyperintense vessels on FLAIR: hemodynamic correlates and response to thrombolysis. *AJNR Am J Neuroradiol* 36:1426–1430
- Goyal M, Menon BK, Derdeyn CP (2013) Perfusion imaging in acute ischemic stroke: let us improve the science before changing clinical practice. *Radiology* 266:16–21
- Donnan GA, Baron JC, Ma H, Davis SM (2009) Penumbra selection of patients for trials of acute stroke therapy. *Lancet Neurol* 8:261–269
- Kim JT, Yoon W, Park MS et al (2009) Early outcome of combined thrombolysis based on the mismatch on perfusion CT. *Cerebrovasc Dis* 28:259–265
- Jovin TG, Liebeskind DS, Gupta R et al (2011) Imaging-based endovascular therapy for acute ischemic stroke due to proximal intracranial anterior circulation occlusion treated beyond 8 hours from time last seen well: retrospective multicenter analysis of 237 consecutive patients. *Stroke* 42:2206–2211
- Inoue M, Mlynash M, Straka M et al (2012) Patients with the malignant profile within 3 hours of symptom onset have very poor outcomes after intravenous tissue-type plasminogen activator therapy. *Stroke* 43:2494–2496
- Lin K, Do KG, Ong P et al (2009) Perfusion CT improves diagnostic accuracy for hyperacute ischemic stroke in the 3-hour window: study of 100 patients with diffusion MRI confirmation. *Cerebrovasc Dis* 28:72–79
- Schellinger PD, Bryan RN, Caplan LR et al (2010) Evidence-based guideline: the role of diffusion and perfusion MRI for the diagnosis of acute ischemic stroke: report of the Therapeutics and Technology Assessment Subcommittee of the American Academy of Neurology. *Neurology* 75:177–185
- Pexman JH, Barber PA, Hill MD et al (2001) Use of the Alberta Stroke Program Early CT Score (ASPECTS) for assessing CT scans in patients with acute stroke. *AJNR Am J Neuroradiol* 22:1534–1542
- Kakeda S, Korogi Y, Hiai Y, Ohnari N, Sato T, Hirai T (2012) Pitfalls of 3D FLAIR brain imaging: a prospective comparison with 2D FLAIR. *Acad Radiol* 19:1225–1232
- Streiner DL, Norman GR (1995) Health measurement scales: a practical guide to their development and use, 2nd edn. Oxford University Press, Oxford
- Jang W, Kwak HS, Chung GH, Hwang SB (2018) Three-dimensional black-blood contrast-enhanced MRI improves detection of intraluminal thrombi in patients with acute ischaemic stroke. *Eur Radiol*. <https://doi.org/10.1007/s00330-018-5323-4>
- Power S, Matouk C, Casaubon LK et al (2014) Vessel wall magnetic resonance imaging in acute ischemic stroke: effects of

- embolism and mechanical thrombectomy on the arterial wall. *Stroke* 45:2330–2334
39. Mandell DM, Mossa-Basha M, Qiao Y et al (2017) Intracranial vessel wall MRI: principles and expert consensus recommendations of the American Society of Neuroradiology. *AJNR Am J Neuroradiol* 38:218–229
 40. Skarpathiotakis M, Mandell DM, Swartz RH, Tomlinson G, Mikulis DJ (2013) Intracranial atherosclerotic plaque enhancement in patients with ischemic stroke. *AJNR Am J Neuroradiol* 34:299–304
 41. Hui FK, Zhu X, Jones SE et al (2015) Early experience in high-resolution MRI for large vessel occlusions. *J Neurointerv Surg* 7:509–516
 42. Storey P, Atanasova IP, Lim RP et al (2010) Tailoring the flow sensitivity of fast spin-echo sequences for noncontrast peripheral MR angiography. *Magn Reson Med* 64:1098–1108
 43. Park J, Kim EY (2010) Contrast-enhanced, three-dimensional, whole-brain, black-blood imaging: application to small brain metastases. *Magn Reson Med* 63:553–561
 44. Knight MJ, McCann B, Tsivos D, Couthard E, Kauppinen RA (2016) Quantitative T1 and T2 MRI signal characteristics in the human brain: different patterns of MR contrasts in normal ageing. *MAGMA* 29:833–842
 45. Lu H, Nagae-Poetscher LM, Golay X, Lin D, Pomper M, van Zijl PC (2005) Routine clinical brain MRI sequences for use at 3.0 Tesla. *J Magn Reson Imaging* 22:13–22
 46. Hohenhaus M, Schmidt WU, Brunecker P et al (2012) FLAIR vascular hyperintensities in acute ICA and MCA infarction: a marker for mismatch and stroke severity? *Cerebrovasc Dis* 34:63–69
 47. Haussen DC, Koch S, Saraf-Lavi E, Shang T, Dharmadhikari S, Yavagal DR (2013) FLAIR distal hyperintense vessels as a marker of perfusion-diffusion mismatch in acute stroke. *J Neuroimaging* 23:397–400
 48. Cheng B, Ebinger M, Kufner A et al (2012) Hyperintense vessels on acute stroke fluid-attenuated inversion recovery imaging: associations with clinical and other MRI findings. *Stroke* 43:2957–2961
 49. Ebinger M, Kufner A, Galinovic I et al (2012) Fluid-attenuated inversion recovery images and stroke outcome after thrombolysis. *Stroke* 43:539–542
 50. Gawlitza M, Gragert J, Quaschling U, Hoffmann KT (2014) FLAIR-hyperintense vessel sign, diffusion-perfusion mismatch and infarct growth in acute ischemic stroke without vascular recanalisation therapy. *J Neuroradiol* 41:227–233
 51. Huang X, Liu W, Zhu W et al (2012) Distal hyperintense vessels on FLAIR: a prognostic indicator of acute ischemic stroke. *Eur Neurol* 68:214–220
 52. Klijn CJ, Kappelle LJ, Algra A, van Gijn J (2001) Outcome in patients with symptomatic occlusion of the internal carotid artery or intracranial arterial lesions: a meta-analysis of the role of baseline characteristics and type of antithrombotic treatment. *Cerebrovasc Dis* 12:228–234
 53. Luo S, Yang L, Wang L (2015) Comparison of susceptibility-weighted and perfusion-weighted magnetic resonance imaging in the detection of penumbra in acute ischemic stroke. *J Neuroradiol* 42:255–260
 54. Dejobert M, Cazals X, Annan M, Debiais S, Lauvin MA, Cottier JP (2016) Susceptibility-diffusion mismatch in hyperacute stroke: correlation with perfusion-diffusion mismatch and clinical outcome. *J Stroke Cerebrovasc Dis* 25:1760–1766
 55. Hermier M, Nighoghossian N (2004) Contribution of susceptibility-weighted imaging to acute stroke assessment. *Stroke* 35:1989–1994